

000
001
002
003
004
005
006
007
008
009
010
011
012
013
014
015
016
017
018
019
020
021
022
023
024
025
026
027
028
029
030
031
032
033
034
035
036
037
038
039
040
041
042
043
044
045
046
047
048
049
050
051
052
053054
055
056
057
058
059
060
061
062
063
064
065
066
067
068
069
070
071
072
073
074
075
076
077
078
079
080
081
082
083
084
085
086
087
088
089
090
091
092
093
094
095
096
097
098
099
100
101
102
103
104
105
106
107

Guided Proofreading of Automatic Segmentations for Connectomics

Supplemental Material

Anonymous ICCV submission

Paper ID 0922

	Traditional Network		Residual Network	
Conv. Layers	2	4	5	13
Dropout Reg.	y	y	y	n
Cost [m]	27.5	383	5080	1094
Test. Acc.	0.925	0.94	0.93	0.90
Prec./Recall	0.93/0.93	0.94/0.94	0.7/0.53	0.74/0.66
F1 Score	0.93	0.94	0.39	0.64
		*		

Table 1: Traditional CNN Architecture versus Residual Network Architecture [1]. All configurations are compared using the same parameters. Our final choice (indicated by *) trains relatively fast and performs better.

Parameter	Search Space
Filter size:	3x3, 5x5, 9x9, 13x13
No. Filters 1:	32, 48, 64
No. Filters 2-4:	32, 48 , 64
Dense units:	256, 512
Learning rate:	0.00001, 0.0001, 0.001, 0.01, 0.03-0.00001
Momentum:	0.9, 0.95, 0.9-0.999
Mini-Batchsize:	10, 100, 128

Table 2: Brute force parameter search for the split error classifier. The final parameters are highlighted.

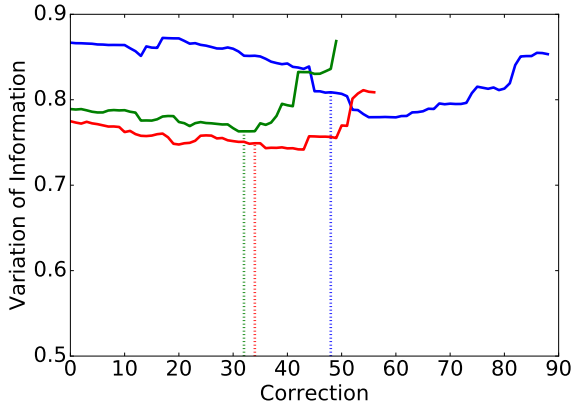


Figure 1: Observations of probability thresholds p_t during automatic selection on three different subvolumes of previously unseen testing data. The dashed lines show when $p_t = 0.95$ is reached.

1. Classifier

1.1. Architecture

We explored different architectures for the convolutional neural network (CNN) for split error detection. We compare traditional CNN architectures versus residual networks [1] (Tab. 1). The traditional architecture with dropout regularization generalized better than residual networks on unseen testing data.

1.2. Training Parameters

We performed a limited brute force parameter search to tune the split error classifier (Tab. 2). This resulted in 3240 different CNN configurations which were evaluated on 10% of our training data. Learning rate and momentum ranges are defined linearly across 2000 epochs.

1.3. Automatic Method Threshold p_t

For automatic selection, we observed a threshold $p_t = 0.95$ as stable when evaluating on previously unseen testing data (Mouse S1 AC3 Open Connectome Project dataset). This means that automatic selection stops once all borders with $p_t \geq 0.95$ were proofread. Figure 1 shows split error

classification on three randomly selected subvolumes ($700 \times 700 \times 2$ voxels) of AC3. In all cases, the threshold $p_t = 0.95$ reduces VI.

108
109
110
111
112
113
114

1.4. Merge Error Detection Pseudo Code

We provide pseudo code on how we detect merge errors to foster understanding of the reported algorithm (Alg. 1). In our experiments, we use $N = 50$ iterations.

Algorithm 1 Merge Error Detection for a label l

```

1:  $l_d = \text{dilate}(l, 20)$ 
2:  $\text{invImage} = \text{invert}(\text{image})$ 
3: for N iterations do
4:    $s_1, s_2 = \text{randomSeedsOnBoundary}(l_d)$ 
5:    $\text{wsImage} = \text{watershed}(\text{invImage}, l_d, s_1, s_2)$ 
6:    $\text{border} = \text{border}(\text{wsImage})$ 
7:    $p = \text{rank}(\text{border})$ 
8:    $p_{\text{merge}} = 1 - p$ 
9: find(max  $p_{\text{merge}}$ )

```

1.5. Limitations

Guided proofreading works on 2D image sections. This enables error correction without a computationally expensive alignment process. However, the output requires an additional (block-)merging step prior to 3D analysis. Several software packages exist for this purpose.

As described in Section 4, the guided proofreading classifier has to be retrained if used on a different species than mouse. In our experiments, parameters did not need to be changed.

2. Automatic Segmentation Pipeline

We create a dense automatic segmentation of electron microscopy data using a combination of a U-net [5] and the GALA agglomeration method [3]. To not bias, these classifiers are trained on different data than GP (Tab. 3).

Training Set U-Net / GALA	Training Set GP	Test Set GP
AC3+AC4 (1024 × 1024 × 175vx)	L. Cylinder (2048 × 2048 × 250vx)	L. Cylinder _{test} (2048 × 2048 × 50vx)
AC4 excl. test (1024 × 1024 × 90vx)	L. Cylinder (2048 × 2048 × 250vx)	AC4 _{test} subvolume (400 × 400 × 10vx)
AC3+AC4 (1024 × 1024 × 175vx)	CREMI A/B/C (1250 × 1250 × 300vx)	CREMI A/B/C _{test} (1250 × 1250 × 15vx)

Table 3: Training data of membrane detection (U-Net / GALA) vs. training data of GP vs. test data.

GALA uses a random forest classifier to agglomerate segments. We use an agglomeration level of 0.3 (after a grid search). We follow the method by Knowles-Barley *et al.* as described in [2].

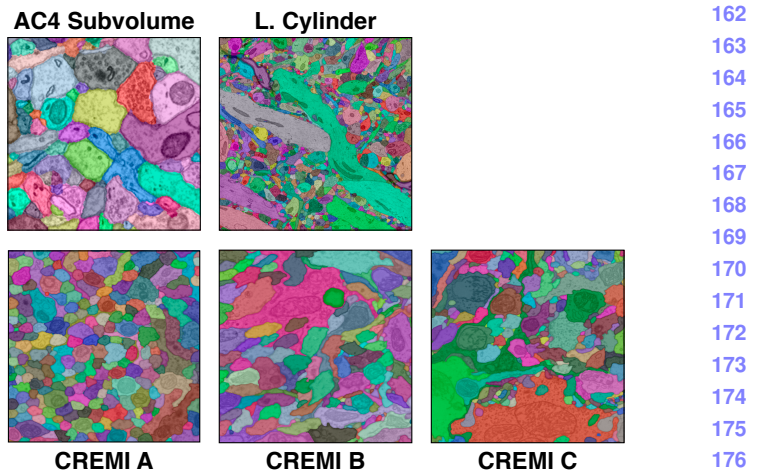


Figure 2: The five different datasets we use for evaluation. The top row shows the first slice of the AC4 and L. Cylinder mouse brain datasets as reported in the paper. The bottom row shows the first slice of the CREMI A/B/C fruit fly datasets which we used for additional experiments.

3. L. Cylinder Results

We report experiments and results on the L. Cylinder dataset in the paper. Figure 3 and 4 visualize the reported results measured as variation of information (VI). We compare automatic selection with threshold and selection oracle using focused proofreading and guided proofreading.

Best possible VI. The selection oracle using guided proofreading does not reach the best possible VI score. We calculate this score by intersecting the initial segmentation and the ground truth. In theory, the classifier should be able to reach this lower bound. However, due to the classification patch size, the membrane probability maps we used included a 30 pixel frame region. Guided proofreading ignores all segments within this frame region, and so cannot reach the best possible VI in some datasets.

4. Additional Experiments

CREMI A/B/C. As part of the MICCAI 2016 challenge on circuit reconstruction from electron microscopy images (CREMI), six ssTEM datasets were made publicly available¹, each $1250 \times 1250 \times 125$ voxels. Since only three datasets include manually-labeled ‘ground truth’, we use these three volumes for our experiments. The volumes are part of an adult fruit fly (*Drosophila melanogaster*) brain. The resolution of all three datasets is $4 \times 4 \times 40 \text{ nm}^3/\text{voxel}$. We evaluate error detection and correction on subvolumes of CREMI A/B/C with the dimensions $1250 \times 1250 \times 5$

¹<http://www.creml.org>

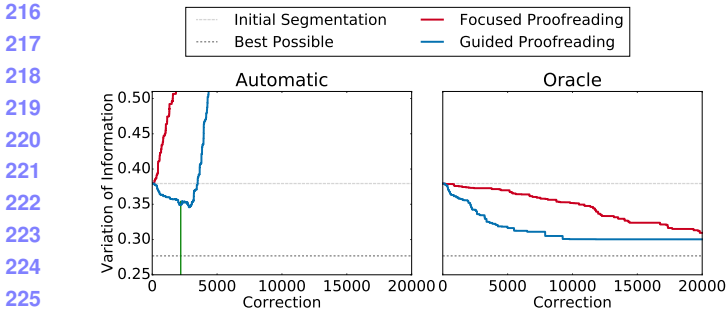


Figure 3: Performance comparison of Plaza’s focused proofreading and our guided proofreading on the L. Cylinder dataset as reported in the paper. All measurements are shown as median VI, the lower the better. We compare automatic selection with threshold ($p_t = 0.95$, green line) and the selection oracle for accepting or rejecting corrections using each method. Guided proofreading yields better results faster with fewer corrections.

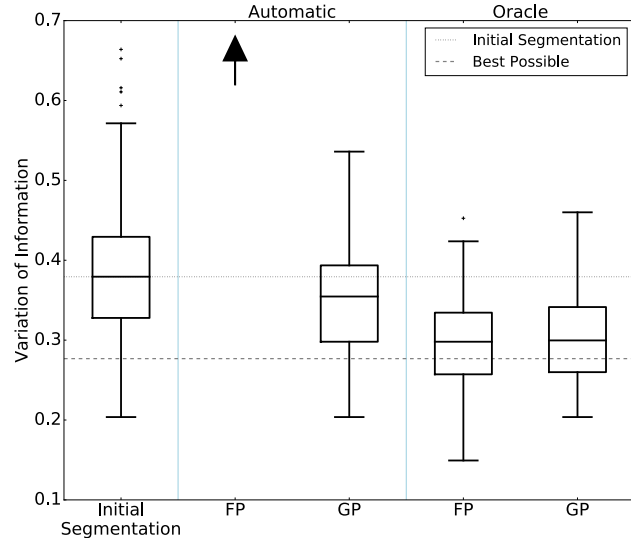


Figure 4: VI distributions of guided proofreading (GP) and focused proofreading (FP) output across slices of the L. Cylinder dataset, with different error correction approaches. The variation resulting from performance of FP with automatic selection is $7.8 \times$ higher than GP (as indicated by the arrow), with median VI of 2.75 and $SD = 0.789$.

voxels. The subvolumes were cut from the last 25 sections of each of the three datasets and unseen during training. We compare focused proofreading and guided proofreading with automatic selection ($p_t = 0.95$) and selection oracle.

Retraining. Since the CREMI data is a different species, we simply retrain our split error classifier as well as focused proofreading by Plaza [4]. For this, we use the first 100

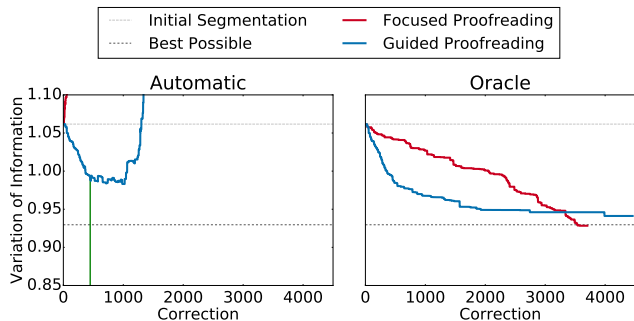


Figure 5: Performance comparison of Plaza’s focused proofreading and our guided proofreading on 5 sections of the CREMI A dataset. All measurements are reported as median VI, the lower the better. The threshold for automatic selection is $p_t = 0.95$ (green line). The slope of the selection oracle shows that guided proofreading reduces VI faster.

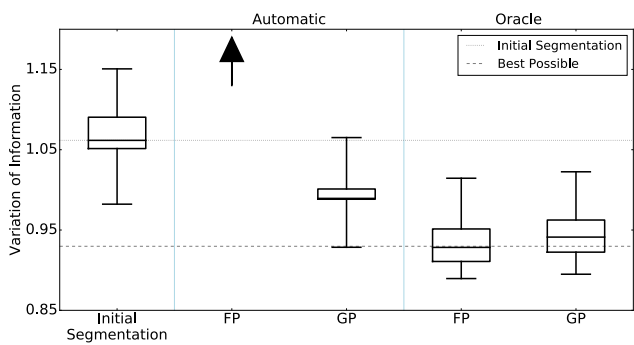


Figure 6: VI distributions of guided proofreading (GP) and focused proofreading (FP) output across slices of the CREMI A dataset, with different error correction approaches. The variation resulting from performance of FP with automatic selection is $5.4 \times$ higher than GP (as indicated by the arrow), with median VI of 5.32 and $SD = 0.009$. GP does not reach the best possible VI as discussed in the text.

sections of each of the three CREMI datasets combined as training data. All parameters are unchanged and left as reported in the paper.

4.1. CREMI A

Figure 5 and 6 compare Plaza’s focused proofreading and guided proofreading on the 5 sections of the CREMI A dataset.

Selection oracle. With focused proofreading, the selection oracle reduces median VI to 0.928, $SD = 0.043$ from an initial median VI of 1.06 ($SD = 0.055$). 532 corrections out of 3707 were accepted. Guided proofreading does not reach the best possible VI, however, reduces VI faster with less corrections to 0.941 ($SD = 0.04$). Out of 4463 corrections,

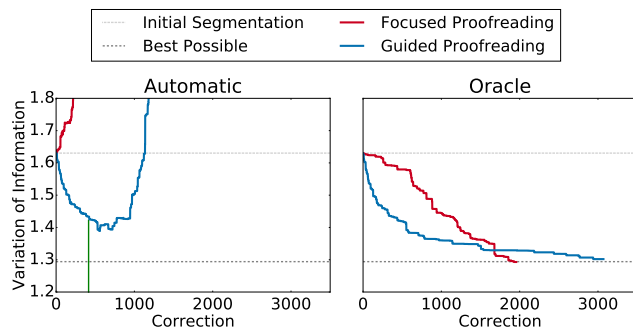
324
325
326
327
328
329
330
331
332
333
334

Figure 7: Split error correction by Plaza’s focused proofreading and our guided proofreading compared on the CREMI B dataset. All measurements are reported as median VI, the lower the better. Automatic selection with threshold (green line) yields reasonable performance using guided proofreading.

341

342
343

1275 were accepted.

344

345

Automatic selection with threshold. Not surprisingly, focused proofreading performs poorly when ran automatically (VI of 5.32, $SD = 0.009$). Guided proofreading is able to reduce VI to 0.989 ($SD = 0.043$) with $p_t = 0.95$.

350

351

4.2. CREMI B

352
353
354

Figure 7 and 8 show the results on the CREMI B dataset.

355

356

357

358
359
360

Selection oracle. Focused proofreading is able to reduce median VI to 1.29, $SD = 0.031$ from an initial median VI of 1.63 ($SD = 0.025$). Out of 1959 corrections, the selection oracle accepted 517. With guided proofreading, the median VI is reduced to 1.30, $SD = 0.03$ while accepting 1111 corrections out of 3073.

361

362

363

Automatic selection with threshold. Focused proofreading results in a VI of 4.25 ($SD = 0.07$). Guided proofreading reduces median VI to 1.43 ($SD = 0.038$).

366

367

4.3. CREMI C

368

369

370

371
372

The results of split error correction using focused proofreading and guided proofreading on the CREMI C subvolume are shown in Figure 9 and 10.

373

374

375

376

377

Selection oracle. With focused proofreading, the initial median VI of 1.75 ($SD = 0.086$) is reduced to 1.45 ($SD = 0.056$) with 670 accepted corrections out of 2694. Guided proofreading is able to reduce the VI to 1.47 ($SD = 0.06$). Here, the oracle accepted 1531 out of 4332 corrections.

378
379
380381
382
383
384385
386
387
388389
390
391392
393
394395
396
397398
399
400401
402
403404
405
406407
408
409410
411
412413
414
415416
417
418419
420
421422
423
424425
426
427428
429
430

431

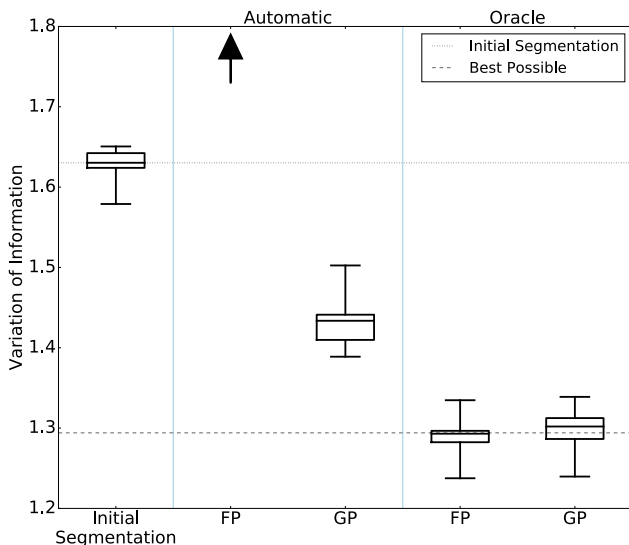


Figure 8: VI distributions of guided proofreading (GP) and focused proofreading (FP) output across 5 sections of the CREMI B dataset. We compare automatic selection and oracle selection. The variation resulting from performance of FP with automatic selection is 3× higher than GP (as indicated by the arrow), with median VI of 4.25 and $SD = 0.07$.

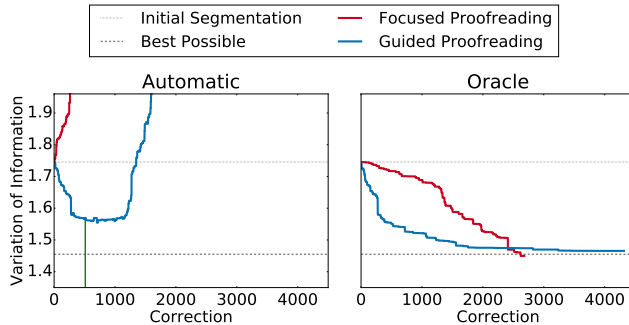


Figure 9: Performance comparison of Plaza’s focused proofreading and our guided proofreading on the CREMI C dataset. Lower VI scores are better. Guided proofreading corrects the initial segmentation faster with less corrections than focused proofreading. The green line shows the automatic threshold $p_t = 0.95$.

Automatic selection with threshold. Focused proofreading results in a VI of 4.81 ($SD = 0.03$). Guided proofreading with $p_t = 0.95$ reduces median VI to 1.57 ($SD = 0.081$).

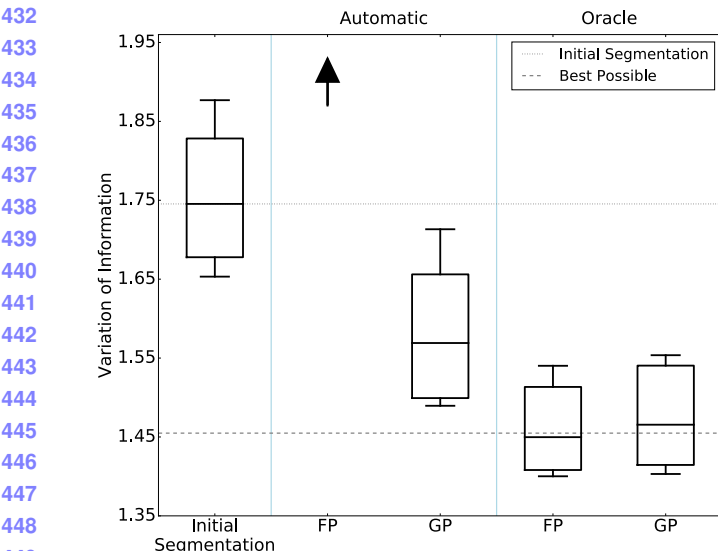


Figure 10: VI distributions of guided proofreading (GP) and focused proofreading (FP) output across the CREMI C subvolume, with different error correction approaches. The variation resulting from performance of FP with automatic selection is 3× higher than GP (as indicated by the arrow), with median VI of 4.81 and $SD = 0.08$.

5. Forced Choice User Experiment

5.1. Recruitment and Participation

Novice participants were recruited via flyer (figure 11). An anonymized listing of all participants including demographic information is shown in table 4.

5.2. Example Classifications

During the user study, participants were asked to accept or reject potential errors and their corrections — some more difficult than others. Figure 13 shows a selection of potential errors and their corrections.

5.3. Subjective Responses

After the experiment, we acquired subjective responses using the NASA-TLX task load index (figure 12). We performed ANOVA to test for statistical significance [6]. Mental, physical, and temporal demands were reported slightly higher for participants using focused proofreading but the analysis did not yield any significance.

- **Mental Demand.** Participants using focused proofreading stated a higher mental demand $M = 11.5$ ($SD = 2.098$) than with guided proofreading $M = 8.1$ ($SD = 2.003$). This was not statistically significant ($F_{1,18} = 3.2574, p = 0.3695$).

- **Physical Demand.** While naturally physical demand



Get **\$10** Cash!
And look at
Pretty Pictures
of the brain while
helping to **Advance**
Science

We are looking for people who are 18+ and have no experience with nano-scale electron microscopy data of neurons (noobs).

The experiment will last less than 1 hour.

Starting NOW!

SIGN UP:

<http://XXX/YYXXXXXXZZZZ>

Contact: Anon. <anon@anon>
Anon.

Figure 11: Participants were recruited with this flyer.

was rated low, participants using focused proofreading stated it slightly higher $M = 5.4$ ($SD = 2.26$) than with guided proofreading $M = 2.9$ ($SD = 1.76$). This was not statistically significant ($F_{1,18} = 1.7507, p = 0.5454$).

- **Temporal Demand.** For temporal demand, participants using focused proofreading $M = 8.4$ ($SD = 1.95$) reported almost equal to guided proofreading $M = 8.3$ ($SD = 1.99$). This was not statistically significant ($F_{1,18} = 0.0033, p = 0.9987$).

- **Performance.** Here, participants were asked to rate their own performance. All participants rated their performance as pretty well (the lower, the better). For focused proofreading $M = 6.8$ ($SD = 1.97$) and for guided proofreading $M = 7.8$ ($SD = 2.04$). This was not statistically significant ($F_{1,18} = 0.3091, p = 0.8878$).

- **Effort.** Participants using focused proofreading stated higher effort $M = 13.0$ ($SD = 2.336$) than with guided proofreading $M = 10.6$ ($SD = 2.127$). This was not statistically significant ($F_{1,18} = 1.1459, p = 0.6599$).

486
487
488
489
490
491
492
493
494
495
496
497
498
499
500
501
502
503
504
505
506
507
508
509
510
511
512
513
514
515
516
517
518
519
520
521
522
523
524
525
526
527
528
529
530
531
532
533
534
535
536
537
538
539

540

NASA Task Load Index

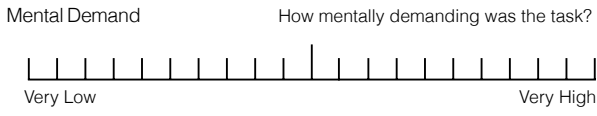
541

Hart and Staveland's NASA Task Load Index (TLX) method assesses work load on five 7-point scales. Increments of high, medium and low estimates for each point result in 21 gradations on the scales.

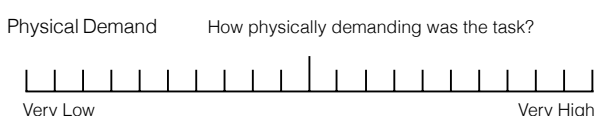
545

Name	Task	Date
------	------	------

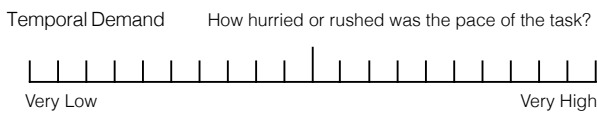
548



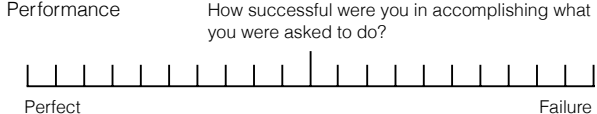
549



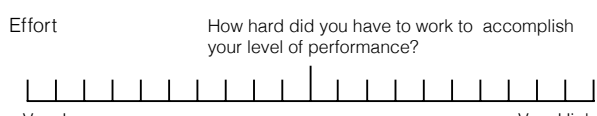
550



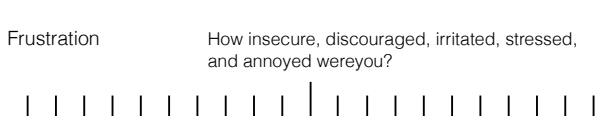
551



552



553



554

Figure 12: The NASA-TLX workload index to record subjective responses.

577

- **Frustration.** Participants overall reported low frustration. Reported were $M = 5.0$ ($SD = 1.90$) using focused proofreading and $M = 5.9$ ($SD = 1.85$) using guided proofreading. This was not statistically significant ($F_{1,18} = 0.3271, p = 0.8818$).

584

References

585

- [1] K. He, X. Zhang, S. Ren, and J. Sun. Deep residual learning for image recognition. In *The IEEE Conference on Computer Vision and Pattern Recognition (CVPR)*, June 2016. [1](#)
- [2] S. Knowles-Barley, V. Kaynig, T. R. Jones, A. Wilson, J. Morgan, D. Lee, D. Berger, N. Kasthuri, J. W. Lichtman, and H. Pfister. Rhoanet pipeline: Dense automatic neural annotation, 2016. (available on arXiv:1611.06973 [cs.CV]). [2](#)
- [3] J. Nunez-Iglesias, R. Kennedy, S. M. Plaza, A. Chakraborty, and W. T. Katz. Graph-based active learning of agglomeration

ID	Sex	Age	Classifier
S38	F	20	FP
S57	F	30	FP
S32	M	38	FP
S34	F	21	FP
S21	F	65	FP
S9	M	33	FP
S45	M	28	FP
S31	M	27	FP
S24	F	21	FP
S6	F	38	FP
S28	M	32	GP
S36	F	19	GP
S35	M	26	GP
S25	M	26	GP
S54	F	30	GP
S53	M	29	GP
S52	M	27	GP
S51	M	31	GP
S200	F	37	GP
S3	F	30	GP

Table 4: The novice participants ($N = 20$) of the forced choice user experiment. The table shows sex (20 female), age ($M = 30$) and the randomly assigned classifier (focused proofreading as FP, guided proofreading as GP).

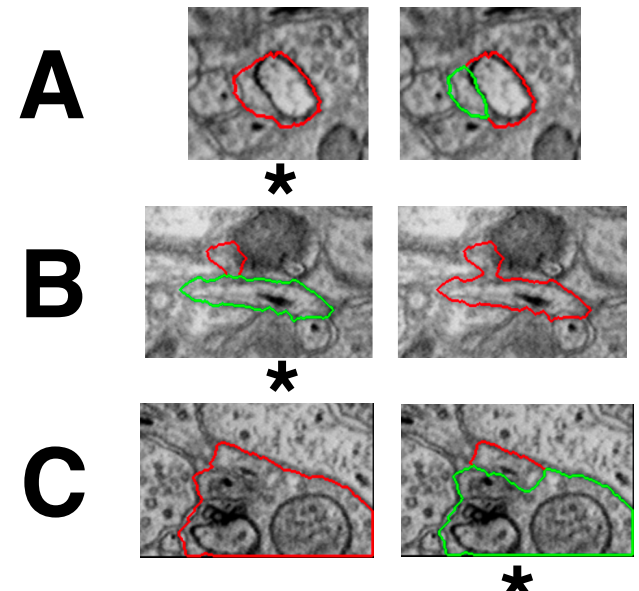


Figure 13: A selection of suggested errors and potential corrections during the forced choice user experiment. The star (*) indicates which choice reduces VI. While all participants were able to correctly choose for patch A, only few were able to correctly choose for patch B and C.

648	(gala): a python library to segment 2d and 3d neuroimages.	702
649	<i>Frontiers in neuroinformatics</i> , 8, 2014. 2	703
650	[4] S. M. Plaza. <i>Focused Proofreading to Reconstruct Neural Con-</i>	704
651	<i>nectomes from EM Images at Scale</i> , pages 249–258. Springer	705
652	International Publishing, Cham, 2016. 3	706
653	[5] O. Ronneberger, P. Fischer, and T. Brox. U-net: Convolutional	707
654	networks for biomedical image segmentation. In <i>Medical Im-</i>	708
655	<i>age Computing and Computer-Assisted Intervention (MICCAI)</i> ,	709
656	volume 9351 of <i>LNCS</i> , pages 234–241. Springer, 2015. (avail-	710
657	able on arXiv:1505.04597 [cs.CV]). 2	711
658	[6] J. P. Shaffer. Multiple hypothesis testing. <i>Annual Review of</i>	712
659	<i>Psychology</i> , 46(1):561–584, 1995. 5	713
660		714
661		715
662		716
663		717
664		718
665		719
666		720
667		721
668		722
669		723
670		724
671		725
672		726
673		727
674		728
675		729
676		730
677		731
678		732
679		733
680		734
681		735
682		736
683		737
684		738
685		739
686		740
687		741
688		742
689		743
690		744
691		745
692		746
693		747
694		748
695		749
696		750
697		751
698		752
699		753
700		754
701		755